

# A novel complexity measure to distinguish organized from disorganized dynamics

Christophe Letellier

Normandie University – CORIA, Avenue de l’Université, F-76800 Saint-Etienne du Rouvray, France

I. Leyva and I. Sendiña-Nadal

Complex Systems Group & GISC, Universidad Rey Juan Carlos, 28933 Móstoles, Madrid, Spain and  
Center for Biomedical Technology, Universidad Politécnica de Madrid, 28223 Pozuelo de Alarcón, Madrid, Spain

(Dated: April 30, 2022)

We propose a new metric to characterize the complex behavior of a dynamical system and to distinguish between organized and disorganized complexity. The approach combines two quantities that separately assess the degree of unpredictability and the lack of structure in the Poincaré plane constructed from a given time series. As for the former, we use the permutation entropy  $S_p$ , while for the later, we introduce a new indicator, the *structurality*  $\Delta$ , which accounts for the fraction of visited points in the Poincaré plane. The complexity measure thus defined as the sum of those two components is validated by classifying in the  $(S_p, \Delta)$  space the complexity of several benchmark dissipative and conservative dynamical systems. As an application, we show how the new metric can be used as a powerful biomarker for different cardiac pathologies.

The past decades have witnessed a considerable growth of the science of complexity, devoted to understand the emerging behavior of collective systems, regardless of their physical, biological, or social nature[1–7]. Much of the research has focused on defining multiple metrics to classify and quantify complex dynamics involving many variables [8]. First attempts were made by extending information theory to dynamical systems [9, 10] and adapting Shannon’s entropy [11] to statistically estimate the apparent randomness present in deterministic chaotic dynamics. As long as the Jaynes’ principle of maximum entropy [12] is properly applied [13–16], the Shannon’s entropy informs about the rate at which information is produced and, consequently, it is a measure of a system’s predictability. However, as Weaver posited [17], there are two classes of complexity: disorganized and organized. While the former can be tackled using the methods of statistical mechanics and probability theory, the latter cannot be fully understood using statistics alone as it involves considerable large number of variables that are interrelated.

Entropic metrics work well as indicators of the level of unpredictability and randomness, but fail to correctly capture the existence of inter-dependencies or structure among the system’s components [18]. For example, it is commonly accepted that both maximally random and perfectly ordered systems do not exhibit any degree of structural organization [18] and, therefore, a measure quantifying their degree of complexity should be minimal [19]. Among several approaches proposed for detecting an underlying structure, are those called *statistical* complexity measures, which account for the graph complexity of the representation of symbolic sequences as trees [18, 20], or in terms of disturbance from the equiprobable distribution of the accessible states of the system [21, 22]. However, these strategies, although using combinations of different indicators, rely on the same background infor-

mation: the probability of different symbolic sequences. Thus, for instance, they are not able to distinguish a fully developed chaos from a stochastic dynamics as in both cases the probabilities are uniform.

In this Letter, we provide a *dynamical* complexity measure  $C_D$  which is able to rank both the degree of the unpredictability and of the structure present in a process. It combines the Shannon entropy as indicator of the unpredictability with the density of points in the Poincaré plane as a novel metric of organization. Our measure is designed to be zero for a fully predictable and perfectly ordered dynamics, the unit for a non-predictable but organized dynamics and a value of two for a non-predictable disorganized one. We illustrate the capabilities of our measure in several dissipative and conservative dynamical systems whose complex behavior can be accessed by tuning a system’s parameter. Finally, we show how it can be used as a biomarker for different cardiac diseases directly obtained from electrocardiogram (ECG) signals.

Let us start by showing how the family of the extensively used entropic based statistical complexity measures  $C_S$ , first introduced by López-Ruiz et al. [21] and later on improved by Martin et al. [22], fails to detect the organized complexity underlying the paradigmatic logistic map.  $C_S$  is usually defined as  $C_S = QH$ , where  $Q$  stands for the so-called disequilibrium, which quantifies how far is the probability distribution of a given process from the uniform one, and  $H$  is the corresponding normalized Shannon entropy. Such a factorization ensures that  $C_S$  vanishes for perfect order ( $H = 0$ ) and maximal randomness ( $Q = 0$ ), and it is expected to capture a wide range of complex behaviors in between. However, when we compare a uniform white noise  $\zeta_n \in [0; 1]$  having a uniform probability distribution, with the logistic map  $x_{n+1} = \mu x_n(1 - x_n)$  whose behavior  $x_n \in [0; 1]$  is controlled by the parameter  $\mu$ , we find a clear example

arXiv:1907.09932v1 [physics.soc-ph] 19 Jul 2019

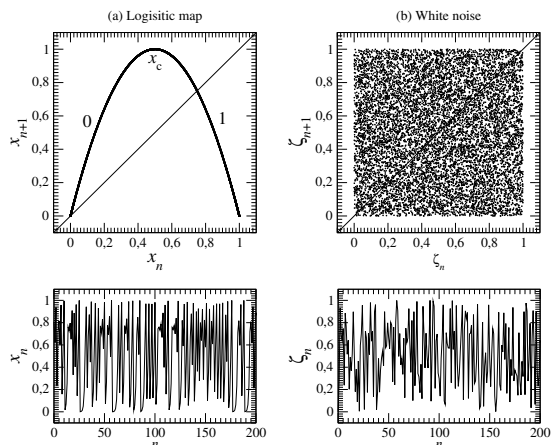


Figure 1. (Upper row) First-return maps for (a) logistic map with  $\mu = 4$  and (b) uniform white noise with the same amplitude. (Bottom row) Characteristic time series for the same both examples. For the logistic map, the first return map shows the generating partition  $x_c = \frac{1}{2}$  and the corresponding symbolic dynamics.

where the statistical complexity measure  $C_S$  is not performing properly, in particular when the logistic map exhibits fully developed chaotic behavior for  $\mu = 4$ . Figure 1 shows an illustrative characterization of the two dynamics by means of first-return maps (top panels) and time series (bottom panels). The time series of both dynamics look quite alike, actually characterized by an almost flat histogram for the symbolic sequences [23], which yields to null values of  $C_S$ . However, their respective first-return maps reveal a well defined underlying structure for the chaotic dynamics (top panel in Fig. 1(a)) while the noise fills the whole available state space (top panel in Fig. 1(b)) with no signs of dynamical organization.

Therefore, we need a marker capable of discriminating the presence of a structured dynamics. The Shannon entropy already quantifies how the structure -when it exists- is visited in the state space. It must be complemented by a second marker capable of measuring how the structure fills the state space, based on the principle that the most structured the attractor is, the smaller the volume it occupies. If we choose the Poincaré section as a more reliable source to compute the entropy than the time series itself [24], then the argument can be reformulated by stating that the smaller the fraction of boxes visited by the Poincaré section, the more constrained and organized the dynamics.

In order to assess how a dynamics is structured in the state space, we introduce the *structurality*  $\Delta$  index, that accounts for the fraction of visited boxes from a partition of the Poincaré plane into  $N_b \times N_b$  boxes, that is,  $\Delta = \sum_{i,j=1}^{N_b} v_{ij} / N_b^2 \in [0; 1]$ , being  $v_{ij} = 1$  if the box  $(i, j)$  contains at least one crossing point and  $v_{ij} = 0$  otherwise. The most sensitive detail in this definition is to specify the partition, the number  $N_b^2$  of boxes and their size  $b_s$ .

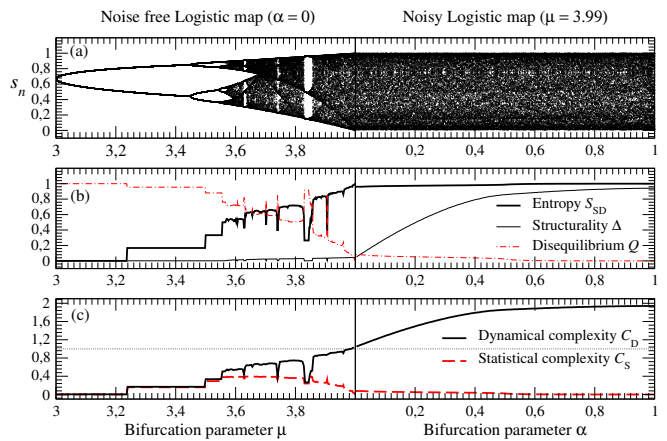


Figure 2. (a) Bifurcation diagram of the logistic map vs  $\mu$  for  $\alpha=0$  (left half) and vs  $\alpha$  for  $\mu = 4$  as it is progressively replaced with noise (right half) according to Eq. (2). (b) Shannon entropy based on the symbolic dynamics  $S_{SD}$  (black thick line), structurality  $\Delta$  (black thin line), and disequilibrium  $Q$  (red dash-dotted line). (c) Dynamical complexity  $C_D = S_{SD} + \Delta$  and statistical complexity  $C_s = S_{SD} \cdot Q$ .  $N_p = 180,000$ .

The former depends on the number  $N_p$  of points in the Poincaré section as  $N_b^2 \sim N_p$  while the later on the size of the Poincaré visited domain as  $b_s = \|\mathbf{x}_{\max} - \mathbf{x}_{\min}\| / N_b$ , being the numerator the maximum distance between any two points in the Poincaré section. A lack of structurality will be evidenced by a large value of  $\Delta$ , while a well ordered dynamics like a period one behavior will have  $\Delta = 1/N_b^2 \sim 0$ .

At this point, we combine into a single dynamical complexity measure  $C_D$  the two components characterizing the lack of predictability, the Shannon entropy  $S_p$ , and the lack of structurality  $\Delta$  as

$$C_D = S_p + \Delta, \quad (1)$$

where  $S_p$  is by default the permutation entropy [25], unless stated otherwise.

We evaluate now how  $C_D$  performs by first discussing its application to the logistic map  $x_n$  coupled to a white noise  $\zeta_n$  as

$$s_n = (1 - \alpha)x_n + \alpha\zeta_n \quad (2)$$

where  $x_n, \zeta_n \in [0; 1]$  and  $\alpha$  is a parameter ranging between 0 ( $s_n = x_n$ , logistic map) and 1 ( $s_n = \zeta_n$ , white noise). Here the Shannon entropy is based on the symbolic dynamics produced by the generating topological partition [24]  $\sigma_i = 0$  if  $s_n < \frac{1}{2}$  and  $\sigma_i = 1$  otherwise, which satisfies the maximum entropy principle for the logistic map [12]. The dynamics is thus reduced to states of 0's and 1's of length 6 whose frequencies of occurrence are calculated over  $N_p = 180,000$ .

The left half of Fig. 2(a) shows the bifurcation diagram of the noise free ( $\alpha = 0$ ) logistic map for  $3 \leq \mu \leq 4$ , while

in the right half  $\mu$  is kept constant to 4 and  $0 \leq \alpha \leq 1$ , giving rise to a fully developed chaos increasingly contaminated by noise of growing amplitude. When computing the dynamical complexity in these two different scenarios using Eq. (1) we find the results displayed in the middle and bottom panels of Fig. 2. In addition to this analysis, we show the corresponding results using a statistical complexity description, adopting the Jensen-Shannon's divergence proposed in [22] as a measure of the generalized disequilibrium.

In Fig. 2(b) we plot the Shannon entropy  $S_{SD}$  (black thick line), the structurality  $\Delta$  (blue thin line) and the generalized Jensen-Shannon disequilibrium  $Q$  (red dash-dotted line).  $S_{SD}$  initially increases in a stepwise form as the logistic map undergoes the period-doubling bifurcation up to a point where a much richer structure arises characterized by chaotic behavior intermingled with periodic windows in which the entropy drops accordingly to the periodicity. For  $\mu = 4$ , the logistic map is fully chaotic, all its symbolic states are equally likely and, therefore,  $S_{SD} = 1$ , reaching the maximum lack of predictability of the system, which keeps bounded independently of the added noise intensity. On the other hand, the structurality  $\Delta$  informs us about how organized is the state space: the Poincaré section of the noise-free logistic map changes from an isolated point for the period-1 cycle ( $\mu = 3$ ) to a smooth unimodal map in the unit square for the fully developed chaos ( $\mu = 4$ , see Fig. 1(a)), yielding in every case to a very well structured dynamics with  $\Delta \ll 1$ , but still capturing the different degrees of chaotic behavior. When noise is added to the  $\mu = 4$  case (left half in Fig. 1(b)),  $\Delta$  increases monotonously until it saturates when the lack of structure fills up completely the unit square and  $\Delta \sim 1$ . Note that, while the entropy barely changes, the structurality is clearly differentiating the increasing degree of disorganization of the dynamics. Regarding the disequilibrium, it behaves as expected as it is again a function of the probability of the different symbolic sequences: it is maximum for period-1 oscillations and vanishes indistinguishably for fully chaotic and stochastic dynamics. Finally, in Fig. 1(c) dynamical (continuous) and statistical (dotted) complexities are depicted together. While  $C_S$  exhibits the well-known behavior exclusively driven by the information contained in the entropy,  $C_D$  is able to discriminate between the different dynamical behaviors in increasing order of complexity, assigning the maximum value  $C_D = 2$  to the fully unpredictable and disorganized dynamics featured by a white noise, the minimum value  $C_D = 0$  to a fully predictable and organized periodic motion, and a value close to 1 for a yet unpredictable but structured chaotic behavior.

So far, we have illustrated the definition of our dynamical complexity measure  $C_D$  using a simple non-linear map. In order to test it in a more general context of flows, we have chosen three dynamical systems whose

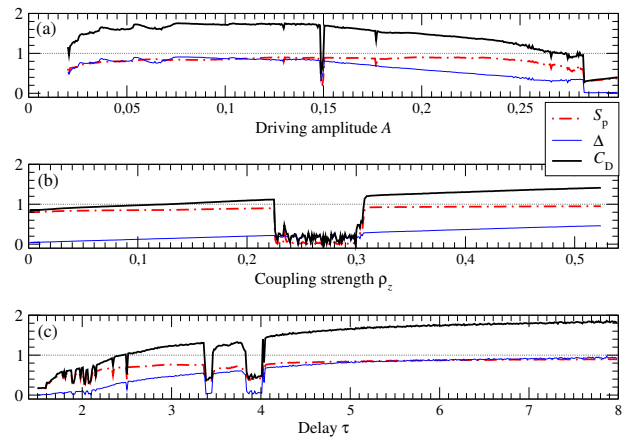


Figure 3. Evolution of the dynamical complexity  $C_D$  versus a bifurcation parameter for (a) the symmetrized double-gyre system, (b) a dyad of Rössler systems and (c) the delay-differential Mackey-Glass equation. The complexity is plotted in black (thick line), the permutation entropy in red (dash-dotted) and the structurality in blue (thin line)

state state range from finite to infinite dimensional and whose dynamical behavior can be controlled by a parameter: (i) a 4D double-gyre conservative system [26], (ii) two coupled Rössler oscillators [27], and (iii) the time delay-differential Mackey-Glass model [28]. Equations, parameters and all the details to calculate  $S_p$  and  $\Delta$  in these systems can be found in the Supplemental Material (SM).

Figure 3 shows the evolution of the dynamical complexity (black thick line) and its two components,  $S_p$  (red dash-dotted line) and  $\Delta$  (thin blue line) vs. the corresponding bifurcation parameter. The first case shown in Fig. 3(a) is a simplified and symmetrized version of the double-gyre model governing geophysical flows [29, 30]. It is considered 2D with a periodic driving of amplitude  $A$  to ensure the mixing. The system is equivalent to a 4D conservative system (see SM) producing chaotic as well as regular behavior in the form of "islands" in a chaotic sea, typically very difficult to describe [26]. It presents high values of the Shannon entropy ( $S_p > 0.7$ ) and structurality ( $\Delta \geq 0.4$ ), revealing that the map is not 1D. The size of the regular islands strongly depends on the  $A$ -value: for instance, when  $A$  increases beyond 0.1488, the size of these islands grows with a consistent decay in the complexity, being  $\Delta$  the most sensitive component to the driving term. In fact, it quantifies the mixing properties of this flow: the larger  $\Delta$ , the greater the mixing.

The next example in Fig. 3(b) is a 6D system of two slightly mismatched chaotic Rössler oscillators diffusively coupled through the  $z$  variable (see SM). This coupling function ensures that synchronization is not attainable for any coupling strength  $\rho_z$  [31]. Therefore,  $S_p$  keeps almost constant and high within the entire coupling interval, except for a window of banded chaos where it drops.

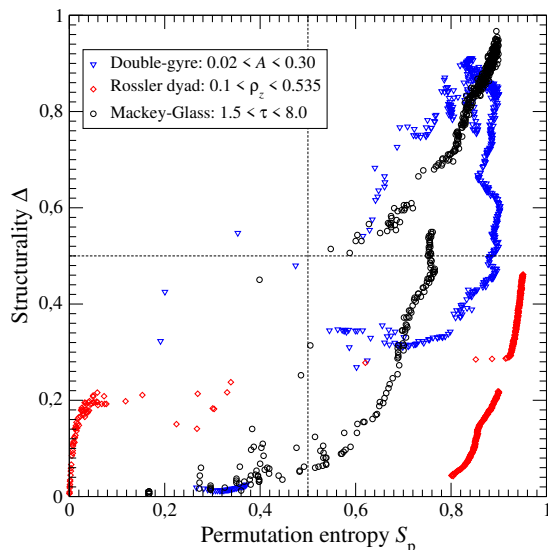


Figure 4. Permutation entropy  $S_p$  versus structurality  $\Delta$  for the same systems and parameters as in Fig.3

The lack of synchronization affects more  $\Delta$ , which slowly increases within the chosen coupling range. In other words, the dynamics does not become less predictable but more difficult to describe.

Finally, let us now consider the Mackey-Glass model whose attractor has an embedding dimension which scales with the delay [28]. In Fig. 3 (c), after an initial period-doubling cascade, the entropy goes up to 0.5 while the structurality is very low in agreement with the establishment of a chaotic attractor with a nearly 1D first-return map. Beyond this point,  $\tau = 2$ , the dynamics becomes more difficult to describe with a much faster growth of the structurality which converges to the entropy.

The results of Fig. 3 are further explored in Fig. 4 plotting the evolution of  $\Delta$  vs  $S_p$  of each system along their respective parameters. Remarkably, the different dynamical regimes are exclusively distributed in three regions according to our complexity descriptor: lower-left region ( $S_p, \Delta < 0.5$ ), corresponding to a very structured and predictable behavior; lower-right region ( $S_p > 0.5, \Delta < 0.5$ ), structured but unpredictable behavior; and upper-right region ( $S_p, \Delta > 0.5$ ) comprising unpredictable and disorganized dynamics.

The applicability of our measure is demonstrated here by using it as a discriminating biomarker for different cardiac dynamics and associated pathologies recorded through electrocardiograms (ECG). The data is fully described in the SM and it is freely available at the PHYSIONET website [32], a research resource for complex physiologic signals. According to a previous study [16], a first-return map based on the  $\Delta RR_n$  (the difference between two successive RR-intervals defined as the duration between two successive R-waves in the ECG, see SM), allows an efficient discrimination between different cardiac

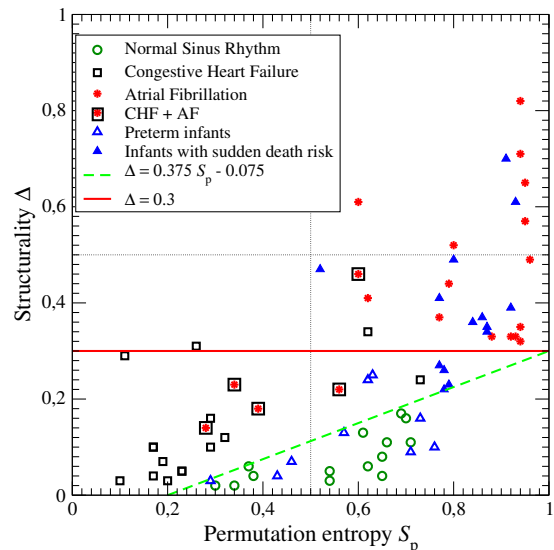


Figure 5. Permutation entropy  $S_p$  vs structurality  $\Delta$  computed for cardiac dynamics data from various groups of patients. Each dot corresponds to a patient and the green dashed line separates healthy (bottom) from non healthy (upper) subjects.

dynamics, using as markers the permutation entropy and an asymmetry coefficient measuring the occurrences of null, positive and negative  $\Delta RR_n$ . Here we replace the asymmetry coefficient by our structurality  $\Delta$ , which is a more general observable by definition.

The results are shown in Fig. 5 where the cardiac dynamics of several populations typically organize around specific areas of the  $S_p - \Delta$  plane. Healthy subjects (green circles) are characterized by small structurality values bounded by  $\Delta < 0.375 S_p - 0.075$  (green dashed line) and  $0.2 < S_p < 0.7$ , which is reflecting that a normal sinus rhythm is irregular due to the variability in the breathing rate and activity of the autonomic nervous system. On the other hand, abnormal rhythms like congestive heart failure (CHF) and atrial fibrillation (AF) have also features clearly distinguishable with our dynamical complexity measure. Patients with CHF (black squares) exhibit well marked segments in the RR sequence associated with ectopic beats characterized by ( $S_p, \Delta$ ) pairs above the straight line  $\Delta > 0.375 S_p - 0.075$  and  $S_p < 0.7$ . Atrial fibrillation (red stars), chaotic activity within the atria which causes the ventricles to contract at seemingly-random intervals, induces structurality  $\Delta > 0.3$  (red continuous horizontal line) and most of them have an entropy  $S_p > 0.7$ , depending on how sustained is the AF. Some intermediate cases (red stars inside black squares) occur when patients present AF combined with ectopic beats. Finally, preterm infants (blue empty triangles) distribute along with the healthy subjects but with slightly higher  $\Delta$  values, while infants diagnosed with sudden death risk have, almost all of them,  $S_p > 0.7$  and  $\Delta > 0.3$ , compatible with an AF case, the

exceptions corresponding to cases developing a mixture of CHF and AF or paroxysmal atrial fibrillation.

We have shown that in order to distinguish between organized and disorganized complexity, a new marker capable of detecting a structured dynamics is needed independently of its degree of predictability. We propose a complexity measure combining these two notions of unpredictability, assessed with a permutation entropy, and that of structurality which quantifies, in a Poincaré section, how the structure underlying a dynamics can be described. The boundary conditions of our new complexity measure are such that it vanishes for regular motion and whose upper limit reflects the disorganized dynamics of an stochastic signal, neither predictable nor easily describable in the Poincaré map. It thus provides a powerful measure for characterizing any stationary dynamics produced by either a map or a flow (as long as the time series can be investigated in a Poincaré plane), dissipative or conservative. As an illustration of its classifying power, we evidenced that this novel complexity measure can discriminate among various groups of common cardiac diseases from the sole measure of an ECG and we are confident that it will be useful for a reliable characterization of a large variety of real-world dynamics.

ISN and IL acknowledge partial support from the Ministerio de Economía y Competitividad of Spain under project FIS2017-84151-P.

- 
- [1] C. Adami, C. Ofria, and T. C. Collier, *Proceedings of the National Academy of Sciences* **97**, 4463 (2000).
- [2] J. S. Perkiömäki, T. H. Mäkikallio, and H. V. Huikuri, *Clinical and Experimental Hypertension* **27**, 149 (2005).
- [3] O. Regev, *Chaos and Complexity in Astrophysics* (Cambridge University Press, 2006).
- [4] M. Sabeti, S. Katebi, and R. Boostani, *Artificial Intelligence in Medicine* **47**, 263 (2009).
- [5] J. C. Flack and D. C. Krakauer, *Chaos* **21**, 037108 (2011).
- [6] A. L. Aquino, H. S. Ramos, A. C. Frery, L. P. Viana, T. S. Cavalcante, and O. A. Rosso, *Physica A: Statistical Mechanics and its Applications* **465**, 277 (2017).
- [7] J. M. Pozo, A. J. Geers, M.-C. Villa-Uriol, and A. F. Frangi, *Journal of Fluid Mechanics* **825**, 704742 (2017).
- [8] S. Lloyd, *IEEE Control Systems Magazine* **21**, 7 (2001).
- [9] A. N. Kolmogorov, *Doklady Akademii Nauk SSSR* **119**, 861 (1958).
- [10] G. Sinai, *Doklady Akademii Nauk SSSR* **124**, 768 (1959).
- [11] C. E. Shannon, *Bell System Technical Journal* **27**, 379 (1948).
- [12] E. T. Jaynes, *Physical Review* **106**, 620 (1957).
- [13] J. Skilling and R. K. Bryan, *Monthly Notices of the Royal Astronomical Society* **211**, 111 (1984).
- [14] A. L. Berger, S. A. D. Pietra, and V. J. D. Pietra, *Computational Linguistics* **22**, 39 (1996).
- [15] R. J. Larivee and S. D. Brown, *Analytical Chemistry* **64**, 2057 (1992).
- [16] E. Fresnel, E. Yacoub, U. Freitas, A. Kerfour, V. Mesager, E. Mallet, J.-F. Muir, and C. Letellier, *Chaos* **25**, 083111 (2015).
- [17] W. Weaver, *American Scientist* **36**, 536 (1948).
- [18] B. A. Huberman and T. Hogg, *Physica D* **22**, 376 (1986).
- [19] D. P. Feldman and J. P. Crutchfield, *Physics Letters A* **238**, 244 (1998).
- [20] J. P. Crutchfield and K. Young, *Physical Review Letters* **63**, 105 (1989).
- [21] H. L. M. R. López-Ruiz and X. Calbet, *Physics Letters A* **209**, 321 (1995).
- [22] M. T. Martin, A. Plastino, and O. A. Rosso, *Physics Letters A* **311**, 126 (2003).
- [23] C. Letellier, *Chaos, Solitons & Fractals* **36**, 32 (2008).
- [24] C. Letellier, *Physical Review Letters* **96**, 254102 (2006).
- [25] C. Bandt and B. Pompe, *Physical Review Letters* **88**, 174102 (2002).
- [26] G. D. Charó, D. Sciamarella, S. Mangiarotti, G. Artana, and C. Letellier, submitted (2019).
- [27] O. E. Rössler and P. J. Ortoleva, *Lecture Notes in Biomathematics* **21**, 67 (1978).
- [28] J. D. Farmer, *Physica D* **4**, 366 (1982).
- [29] S. C. Shadden, F. Lekien, and J. E. Marsden, *Physica D* **212**, 271 (2005).
- [30] C. Coulliette and S. Wiggins, *Nonlinear Processes in Geophysics* **7**, 59 (2000).
- [31] S. Boccaletti, V. Latora, Y. Moreno, M. Chavez, and D.-U. Hwang, *Physics Reports* **424**, 175 (2006).
- [32] A. L. Goldberger, L. A. N. Amaral, L. Glass, J. M. Hausdorff, P. C. H. Ivanov, R. G. Mark, J. E. Mietus, G. B. Moody, C.-K. Peng, and H. E. Stanley, *Circulation* **101**, e215 (2000).